Improving the Transient Stability by Modifying the Power Exchange by the HVDC Transmission

Teja Bandaru, Ujjwal Dhawa, Dheeman Chatterjee and Tanmoy Bhattacharya

Dept. of Electrical Engg.,
Indian Institute of Technology Kharagpur, India.
tejaeee54@gmail.com

Abstract—The high voltage direct current (HVDC) transmission can significantly influence the transient stability of the power system to which it is connected. This work carries an investigation in which the active and reactive powers exchange by the HVDC converter with the system are modulated to improve the transient stability. For this study, a point to point (PTP) HVDC system connected to WSCC 3 machine 9 bus system is considered. The topology of the HVDC converters are considered to be hybrid modular multilevel converters (MMCs). The simulations are performed on PSCAD/EMTDC platform.

Keywords—Power system, Modular multilevel converters, HVDC transmission, Transient stability.

I. INTRODUCTION

The high voltage direct current (HVDC) transmission is considered as a flexible and efficient high power transmission medium over long distances [1]-[3]. For many years, the line commutated converters (LCCs) made the realization of the high power HVDC converters [1]. In recent years, the voltage sourced converters (VSCs) are emerged as the HVDC converters due to their various advantages (such as less filter requirement, no requirement of additional reactive power support and etc) over the LCCs [4]. The modular multilevel converter (MMC) is perceived as the prominent VSC topology in HVDC transmission due to its modularity, scalability and etc [5]. The half-bridge submodule (SM) based MMC (HB-MMC) and full-bridge MMC (FB-MMC) are the basic configurations of the MMC. In the HVDC application, both of these topologies have their own advantages as well as disadvantages. For e.g., HB-MMC is simple and economic converter topology; however, it does not provide dc fault current blocking capability. Though FB-MMC can interrupt the dc fault current, it does at the cost of increased semiconductor switches and hence increased cost and the losses. The hybrid MMC topology, which is the combination of both HB and FB SMs, is an optimum converter topology which can address the above issues [6]-[7].

The VSC can independently control the active and reactive powers injected into the power system. During normal conditions, the energy control center decides the power to be transferred over the dc link, while the remaining power capacity at each converter can be utilized to regulate the voltage magnitude at its ac bus [8]. During the disturbances, such as ac faults etc., the active and reactive powers can be modulated to improve the stability and also to improve the damping of the power oscillations. In a conventional VSC

based HVDC, the active and/or reactive powers are modulated to improve the damping of power system oscillations after being subjected to ac faults [9]. It is found that, modulating active power improves the damping much (around four times) compared to modulating only reactive power [9]. A study on power oscillations damping by modifying both active and reactive powers of the VSC-HVDC using a decentralized control approach is presented in [10]. In [11], a comparison between the LCC-HVDC and VSC-HVDC in the improvement of transient stability and the oscillations damping is presented. In [12], improvement of power system stability with the use of VSC-HVDC link compared with the use of HVAC link is presented. Using the information of critical clearing times without modulating the powers, optimal locations of VSC-HVDC in the Belgium grid are analyzed in [13]. Power system stability and oscillations damping improvement using the global measurements and the model predictive control for the modifying the VSC-HVDC powers in the European power grid is analyzed in [14]. The active power of the VSC-HVDC connected to wind farms is modified during the post fault for improving the transient stability of the power system [15]-[16].

In this work, a similar investigation has been carried out to study the effect of the active and/or reactive powers modulation of the MMC-HVDC on the improvement of the transient stability of the power system. For this a point to point (PTP) HVDC transmission system is considered which connects two asynchronous ac systems. Among these, one of the ac systems is considered to be WSCC 3 machine 9 bus system and the other being a stiff grid. Also, the control structure used for the MMC based HVDC system is presented.

II. MODELING OF THE POWER SYSTEM AND CONTROL OF THE MMC BASED HVDC SYSTEM

A. Modeling of the power system

In this work, the power system loads are modelled as constant impedance. The synchronous generators are represented using the flux-decay model and with the static exciters as given below [17].

$$\dot{\delta}_i = \Delta\omega_i \tag{1}$$

$$\dot{\Delta\omega}_i = \frac{\omega_s}{2H_i}(P_{mi} - P_{ei} - K_{di}\Delta\omega_i) \tag{2}$$

$$\dot{E}'_{qi} = \frac{1}{T_{doi}}\left[-E'_{qi} - (x_{di} - x'_{di})I_{di} + E_{fdi}\right] \tag{3}$$
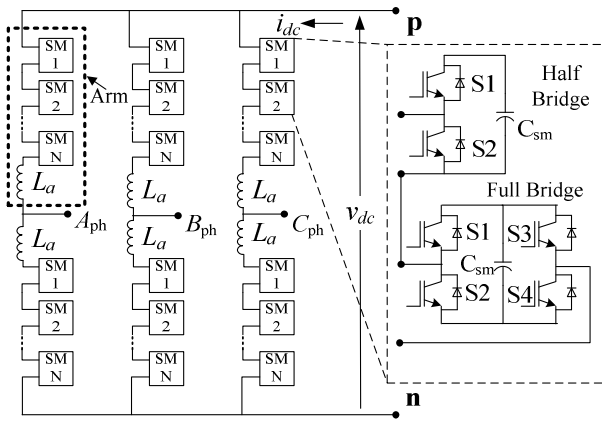
Fig. 1. Hybrid MMC topology.

$$\dot{E}_{fdi} = \frac{1}{T_{Ai}}\left[-E_{fdi} + K_{Ai}\left(V_{refi} - V_{ti}\right)\right] \quad (4)$$

where, $P_{ei} = E'_{qi}I_{qi} + \left(x_{qi} - x'_{di}\right)I_{di}I_{qi}$;

$$I_{di} = \frac{E'_{qi} - V_{ti}\cos(\delta_i - \theta_i)}{x'_{di}}; \quad I_{qi} = \frac{V_{ti}\sin(\delta_i - \theta_i)}{x_{qi}}$$

$i = 1, 2, \ldots, m.$ (m is number of alternators)

Here, δ is the rotor angular position, $\Delta\omega$ is the rotor speed deviation (in rad/sec), ω_s is the synchronous speed in rad/s, H is the inertia constant in MJ/MVA, K_d is the damping coefficient, P_m is the mechanical power in p.u., P_e is the electrical power output in p.u., E'_q is the q-axis component of transient internal voltage, V_t and θ are the voltage and its angle at the terminal of the alternator, V_{ref} is the reference for V_t, x_d and x_q are the direct-axis and quadrature-axis synchronous reactances respectively, x'_d and x'_q are the d-axis and q-axis transient reactances respectively, T'_{do} is the direct-axis open circuit time constant, E_{fd} is the voltage of the exciter, K_A and T_A are the static exciter gain and its time constant respectively.

B. Hybrid MMC based HVDC and its control

Fig. 1 shows the topology of the hybrid MMC [18]. For a given nominal direct voltage (V_{dcn}) and nominal direct current (I_{dcn}), the choice of number of SMs in each arm (N) depends on the nominal capacitor voltage (V_{cn}) and the ac modulation index (k_{MMC}) and is calculated as in (5). In order to limit the dc fault current by the hybrid MMC without blocking the gate

pulses of the SMs, the minimum dc voltage (V_{dcmin}) that the MMC has to generate is to be specified (usually less than or equal to zero). This enables the converter to exchange reactive power during the dc fault. The required number of HB- and FB-SMs can be calculated from the information of V_{dcmin}, k_{MMC}, V_{cn} and V_{dcn} [7]. In this work, 80% of the SMs are considered to be FB-SMs.

$$N = (k_{MMC}V_{dcn} + V_{dcn})/(2V_{cn}) \quad (5)$$

Fig. 2 shows the schematic diagram of PTP-HVDC transmission system having hybrid MMCs. Through a transformer, each MMC is connected to its AC grid at the point of common coupling (PCC). The DC terminals of both the MMCs are connected through an overhead HVDC transmission line represented using lumped 'T' model [19]. The information of the HVDC system parameters is shown in the Appendix. The schematic diagram of the control structure of the hybrid MMC based HVDC system is shown in Fig. 3. The ac side controllers are realized using synchronously rotating reference (*d-q*) frame [8]. As shown in the figure, the active power (P_g) and reactive powers (Q_g) exchange by the MMC with the ac grid are controlled through *d*-axis current (i_d^*) and *q*-axis current (i_d^*) respectively. The average value of SM capacitor voltages of the MMC (V_{cav_tot}) can be regulated through i_d^*. In this work, during normal operation both the MMCs are selected to regulate V_{cav_tot} through i_d^* by positioning the selector switch 'S_d' at 0. Similarly, the ac voltage magnitude at the PCC can be regulated using i_q^* and by positioning the selector switch 'S_q' at 0, else the MMC injects fixed reactive power (Q^*) into the ac grid. The dc current (I_{dc}) controller (in Fig. 3) regulates the dc current injected by the MMC into the HVDC line by varying the inserted leg voltage (v_{leg}). The I_{dc}-controller can be used either regulate the dc power (P_{dc}) to its reference or can be used to regulate the V_{cav_tot} and can be selected with the help of the selector switch 'S_{dc1}'. During the normal conditions active power is regulated through I_{dc} by S_{dc1} positioning at '0'. In a PTP-HVDC system, one converter regulates the power in the dc link (termed as *P*-setting terminal), while the other converter regulates the dc link voltage (V_{dc}-setting terminal). This mode of the operation of the MMC can be selected using the selector switch 'S_{dc2}' in Fig. 3. Positioning S_{dc2} at '1' makes the MMC to become V_{dc}-setting terminal; whereas, positioning at '0' makes it to become *P*-setting terminal. In this work, MMC-1 (in Fig. 2) is operated as V_{dc}-setting terminal and the MMC-2 as *P*-setting terminal. The ac voltage references from the ac side controllers (e_A^*, e_B^*
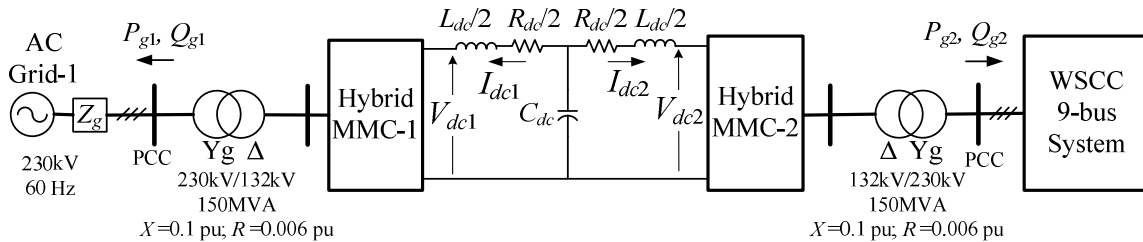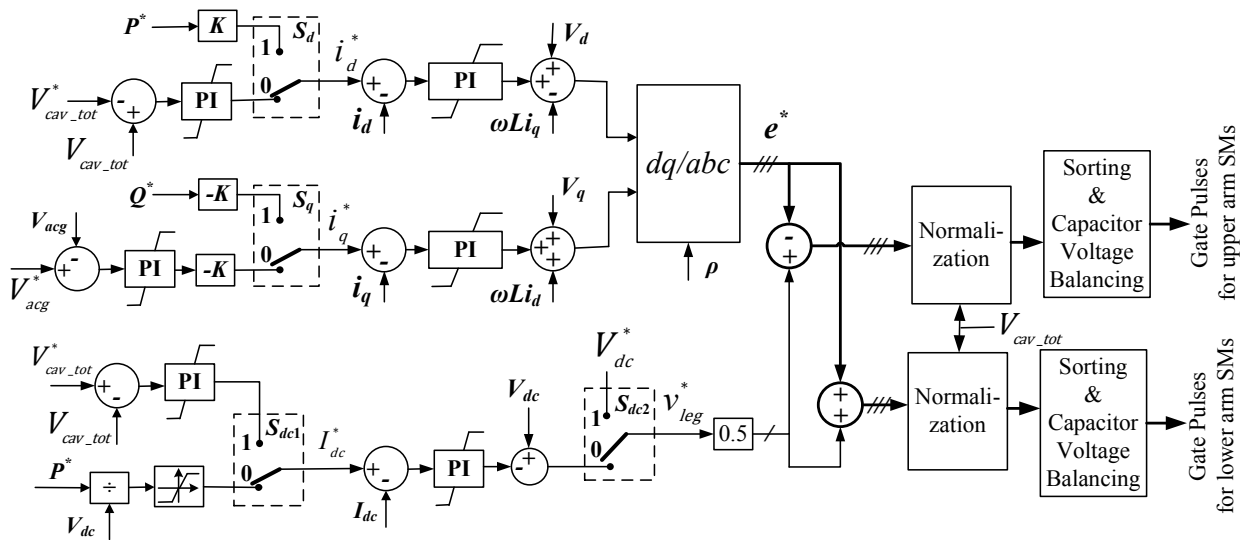

Fig. 2. Hybrid-MMC based PTP-HVDC system.

Fig. 3.Schematic diagram of control structure of the MMCs.

and e_C^*) are subtracted/added from/to the half of the inserted leg voltage reference (v_{leg}^*) to get the upper/lower arm voltage references of the respective phases. Further, these references are normalized with the V_{cav_tot} and the outputs of the normalization block are processed to the 'Sorting and capacitor voltage balancing' algorithm. Using the nearest level control (NLC) and the suitable capacitor voltage sorting methods, the algorithm generates the firing pulses for the switches in the arms [7].

III. TEST SYSTEM AND THE TEST CASES

The schematic diagram of the WSCC 3 machine 9 bus system considered in this work is shown in Fig. 4 [17]. MMC-2 of the PTP-HVDC system (in Fig. 2) is connected to WSCC 9 bus system at one of the load buses (5, 6 and 8). The other converter (MMC-1) is considered to be connected to a strong ac grid (termed as AC Grid-1 in Fig. 2) which is represented using its Thevenin's equivalent. It is considered that the short circuit ratio (SCR) and the inertia of the AC Grid-1 are higher, so that any larger variations in the dc link power can be absorbed by the inertia of AC Grid-1. In WSCC 9-bus system, an additional load of 100MW is connected as local load at the bus to which the HVDC system is connected. During normal operating conditions HVDC system feeds this local load.
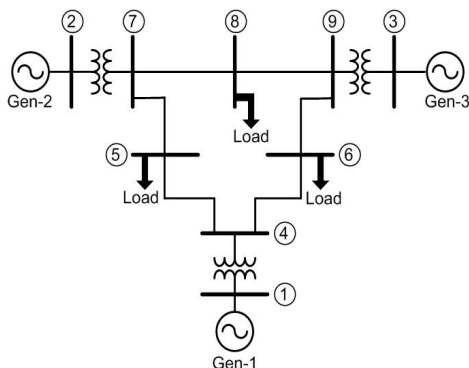

Fig. 4. Schematic diagram of WSCC 3 machine 9 bus system.

TABLE I. TEST CASES

Condition		Case-(a)	Case-(b)	Case-(c)
During fault	P^*	zero	zero	zero
	Q^*	zero	zero	modified
Post fault	P^*	prefault value	modified	modified
	Q^*	zero	zero	modified

In order to investigate the improvement of the transient stability of the power system when HVDC is connected, three cases are considered in this work as given in Table I. As shown in the table, the active power reference of MMC-2 (P^*) (positive sign is assigned for P^* when flowing from MMC-2 to 9-bus system) is made zero during the fault for all the cases; whereas, it is restored to pre-fault value for case-(a) and it is modified based on the frequency error for the cases (b) and (c). Similarly, the reactive power reference (Q^*) is made zero for the cases (a) and (b); whereas, it is modified for case-(c) to regulate the ac bus voltage. For the cases (b) and (c), the active power reference of the MMC-2 is modified by using the P-I controller as shown in Fig. 5. As shown in the figure, the measured frequency at the PCC (f_{PCC}) is compared with its reference (f^*) and the error is given as input to the P-I controller. The P-I controller output, which is modulating power reference (P_f), is added to the P_{ref} of the converter to get the modified active power reference (P^*). As shown in Fig. 5, a selector switch 'S_f' is used to choose the option of modulating the active power during the post fault. For case-(a), S_f is positioned at '0'; whereas, for the cases (b) and (c) it is positioned at '1'. The limits on the P_f are considered to be ±50MW (0.5 pu) in case-(b) and ±30MW (0.3 pu) in case-(c).
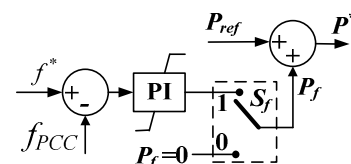

Fig. 5.Controller for modulating the active power reference.

In case-(c), the remaining available capacity of the MMC $\left(\text{i. e., } \sqrt{S_{mmc}^2 - (P^*)^2}\right)$ is used as the limits for the reactive power modulation. In this work, the suitable K_P and K_I values for the power modulating controller (in Fig. 5) are found out using off-line study and are given as 1 MW/Hz and 2500 MW/Hz-s respectively [15].

IV. RESULTS AND DISCUSSION

In this work, the transient stability study is carried out by applying 3-phase short circuit faults at different buses (each at a time) of the WSCC 9 bus system. The faults are considered to be self-clear in nature. At first, the study is carried out for the PTP-HVDC system (MMC-2) connected at bus 5 of the WSCC system (in Fig. 4). An additional load of 100MW is added at bus 5 which is supplied by the MMC-2 (i.e, P_{ref} = 100MW) at unity power factor (UPF). Thus during pre-fault condition, the alternators does not supply any active power to this additional load. The transient stability assessment is made by finding the critical clearing times (t_{cr}). The simulations are performed on PSCAD/EMTDC platform for the three cases in Sec III (Table I).

1. Transient stability results for with and without modulating P* and UPF operation

Here, the transient stability study is carried out for case-(a) (i.e., with P^* maintained to the pre-fault value during post fault), and case-(b) (i.e., with modulating P^* based on the frequency). In both of these cases the MMC reactive power is made zero. Initially, the simulation of the WSCC system having connected HVDC and supplying the additional load is carried out for some duration. After being established steady state, a 3-phase short circuit fault is applied at bus 5 of the system for a duration 545 ms. The results for the two cases are shown in Fig. 6. As shown in the figure , the fault is applied at t = 0.5s. Fig. 6(a) shows the variations of the rotor angle of Gen-2 with respect to the reference machine (Gen-1) for the two cases. It can be seen that, the system becomes unstable for the case in which P^* is restored to pre-fault value (case-a). This is due to the fault duration (545 ms) is higher than its t_{cr} (534 ms). However, by modulating the P^* based on the local measured frequency (case-b), the system is made stable. During the fault, as the mechanical power input to the alternators does not change fast, the reduction in electrical power accelerates the machines and hence the frequency also increases. So, in case-(b), as the P^* is modulated based on these variations in the frequency, the power injected by the HVDC is varied which helps in improving the stability. During acceleration of the machines, the HVDC injects less power into the system; whereas, during deceleration it injects more power. It is considered that, the inertia of the ac grid in the other side of the HVDC system (AC Grid-1) is high enough, so that it can absorb the larger variations in the active power due to modification in P^* and retains its stability. The variations of Gen-2 output power for the two cases are shown in Fig. 6(b). Also, the variations in the active power of the MMC-2 for the two cases are shown in Fig. 6(c). It can be seen that, during first swing in the post fault, the MMC-2 power is regulated close to its pre-fault value (1.0 pu) in case-(a); whereas, it is modulated in case-(b). The corresponding modulating power reference (P_f) for the case-(b) is shown in Fig. 6(d). It should
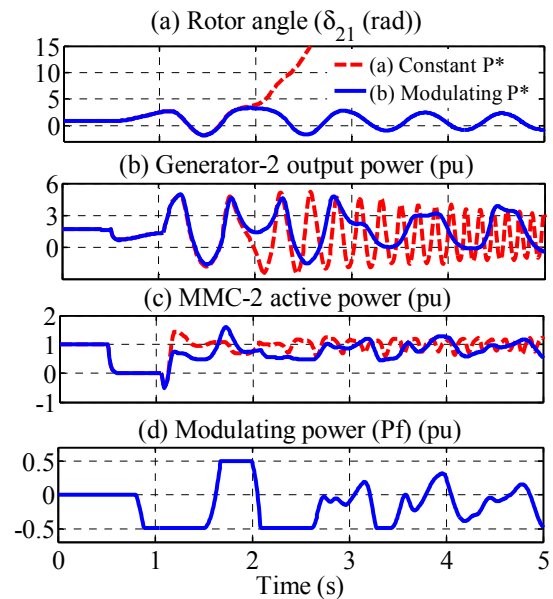

Fig. 6. Transient stability results for case-(a) and case-(b).
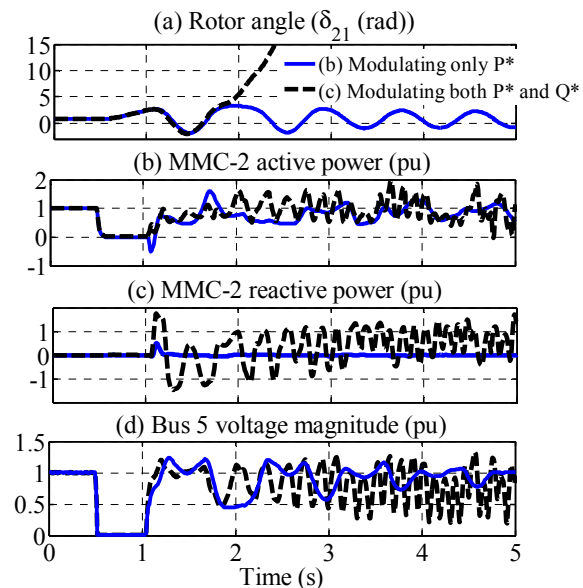

Fig. 7. Transient stability results for case-(b) and case-(c).

be noted that, throughout this study the reactive power reference (Q^*) of the MMC is made zero. Now, the study is further extended by varying Q^* in order to regulate the ac voltage magnitude at bus 5.

2. Transient stability results with modulation of both P* and Q*

As similar to the previous cases, in this case also the fault is applied at bus 5 for the duration of 545 ms. Fig. 7(a)–Fig. 7(d) shows the variation of the rotor angle, active power of the MMC, reactive power of the MMC, and the voltage magnitude at bus 5 respectively for the cases, only P^* is modulated (case-b), and both P^* and Q^* are modulated (case-c). It can be seen that, the stability is deteriorated in the case of both the powers are modulated. This is due to, as compared to case-(b), the limits on the P_f is reduced in case-(c) to increase the reactive

power capability. Also, as the constant impedance loads are considered here, the higher values of the ac voltage magnitudes in case-(b) (>1.0pu) during the first swing of the system increases the power consumed by the loads and hence reduces the acceleration power of the alternators compared to case-(c) in which the voltages are regulated close to 1.0 pu.

The t_{cr} values for the three cases and for various fault locations are shown in Table II. For comparison, the t_{cr} values for the base case (i.e., without connecting the HVDC and additional load) are also specified. It can be observed from the table that, the t_{cr} values for the three cases (a, b and c) are significantly improved compared to the base case for the faults at bus 4 and 5. However, the improvement in t_{cr} values is not significant for the faults at the remaining buses. Further, it can be observed that, the t_{cr} values in case-(b) either higher (for buses 4 & 5) or equal to the t_{cr} values in case-(a). It indicates that, modulating P^* (case-(b)) improves the transient stability compared to maintaining P^* constant (case-(a)) during the post fault. However, the t_{cr} values for all the buses (except bus 4) in case-(c), are less than the t_{cr} values in case-(b) which indicate modulation of both P^* and Q^* worsens the transient stability compared to modulating only P^*. Hence it can be concluded from the table that for the system with constant impedance loads, modulating only active power of the HVDC improves the transient stability significantly.

TABLE II. CRITICAL CLEARING TIMES FOR HVDC CONNECTION AT BUS 5

Faulted bus no.	t_{cr} (ms)			
	Base case	Case-(a)	Case-(b)	Case-(c)
4	335	358	367	399
5	480	534	558	508
7	248	239	239	219
8	371	376	378	366
9	266	265	264	237

Next, the studies are carried out for the cases of HVDC connected at bus 6 and bus 8 and the t_{cr} values obtained for different fault locations for these two HVDC connections are presented in Table III and Table IV respectively. Similar variations in the t_{cr} values (as in the case of HVDC connection at bus 5) can be observed for these two HVDC connections. Hence, irrespective of the bus to which the HVDC is connected, the case in which only the active power of the MMC is modified improves the transient stability of the power system significantly.

TABLE III. CRITICAL CLEARING TIMES FOR HVDC CONNECTION AT BUS 6

Faulted bus no.	t_{cr} (ms)			
	Base case	Case-(a)	Case-(b)	Case-(c)
4	335	376	393	434
5	480	565	617	-
7	248	234	234	217
8	371	377	388	342
9	266	270	270	233

TABLE IV. CRITICAL CLEARING TIMES FOR HVDC CONNECTION AT BUS 8

Faulted bus no.	t_{cr} (ms)			
	Base case	Case-(a)	Case-(b)	Case-(c)
7	248	235	236	241
8	371	405	385	422
9	266	238	285	237

CONCLUSION

It can be concluded that, by modifying the power exchange of the MMC-HVDC system with its connected ac grid the transient stability can be improved. For the power system having constant impedance loads, modifying only the active power output of the MMC connected to power system improves the transient stability significantly compared to the case in which both active and reactive powers are modified. Also, this statement is valid irrespective of the location of the HVDC connection in the power system.

APPENDIX

WSCC 9 bus system (Fig. 4) data is given in [17]. (Base MVA = 100, Base voltage = 230kV).

Parameters of MMC-HVDC system (Fig. 2):

Parameters	Specifications
AC Grid-1	
Rating	230kV (L-L), 60Hz.
Transformer	
Rating, Leakage reactance and resistance	150MVA, 230kV/132kV (Yg/Δ) 0.10 p.u and 0.006 p.u. respectively
Hybrid MMCs	
Rated power and AC Voltage	150MVA, 132 kV (L-L)
Rated DC voltage (V_{dcn})	200kV
Number of SMs per arm (N)	70
Number of HBSMs per arm (N_{HB})	14
Number of FBSMs per arm (N_{FB})	56
Nominal capacitor voltage (V_{cn})	3.5kV
SM capacitance (C_{sm})	5mF (Time constant of 50kJ/MVA)
Inductance of arm reactor (L_a)	0.0308H. (0.10 p.u.)
Resistance of arm reactor (R_a)	0.508Ω (0.005 p.u.)
HVDC Line (Overhead)	
Rating	120MW, 200kV
R_{dc}, L_{dc} and C_{dc}; (length)	2.75Ω, 0.115H and 1.0μF; (50km)

REFERENCES

[1] Kimbark E. W., "Direct current transmission", 1st ed., Wiley-Interscience pub., New Jersey, USA, 1971.

[2] Arrillaga J., "High voltage direct current transmission", 1st ed., Peter Peregrinus Ltd., London, UK, 1983.

[3] K. R. Padiyar, "HVDC power transmision systems", 3st ed., New Age International pub., India, 2017.

[4] Flourentzou, N., Agelidis, V.G., Demetriades, G.D., "VSC-Based HVDC Power Transmission Systems: An Overview", *IEEE Trans. on Power Electronics,* vol. 24, no. 3, pp.592-602, 2009.

[5] A. Lesnicar and R. Marquardt, "An innovative modular multilevel converter topology suitable for a wide power range," in *Proc. of IEEE PowerTech*, Bologna, Italy, June 23-26, 2003.

[6] V. Hofmann and M. M. Bakran, "Optimized design of a hybrid-MMC and evaluation of different MMC topologies," *18th European Conference on Power Electronics and Applications (EPE'16 ECCE Europe)*, Karlsruhe, pp. 1-9, 2016.

[7] Lin, W., Jovcic, D., Nguefeu, S., & Saad, H., "Full-Bridge MMC Converter Optimal Design to HVDC Operational Requirements," *IEEE Trans. on Power Delivery*, vol. *31, no.*3, 1342-1350.June 2016.

[8] Yazdani A., Iravani R., (2010), Voltage-Sourced Converters in Power Systems, 1st ed., Weley pub., New Jersey, USA.

[9] Thorburn, Stefan & Rudervall, Roberto & Asplund, Gunnar & Jansson, Erik, "Power system stability benefits with VSC DC-transmission systems", CIGRE, B-4, 2004.

[10] Y. Pipelzadeh, B. Chaudhuri and T. C. Green, "Control Coordination Within a VSC HVDC Link for Power Oscillation Damping: A Robust Decentralized Approach Using Homotopy," in *IEEE Transactions on Control Systems Technology*, vol. 21, no. 4, pp. 1270-1279, July 2013.

[11] Hu Zhaoqing, Mao Chengxiong and Lu Jiming, "Improvement of transient stability in AC system by HVDC Light," *2005 IEEE/PES Transmission & Distribution Conference & Exposition: Asia and Pacific*, Dalian, 2005, pp. 1-5.

[12] H. F. Latorre and Ghandhari M., Hu Zhaoqing, "Improvement of power system stability by using a VSC-HVdc," *Electrical Power and Energy Systems*, Vol. 33, pp. 332-339, 2011.

[13] F. Leung Shun, R. Muhamad, K. Srivastava, S. Cole, D. Van Hertem and R. Belmans, "Influence of VSC HVDC on transient stability: Case study of the Belgian grid," *IEEE PES General Meeting*, Providence, RI, 2010, pp. 1-7.

[14] A. Fuchs, M. Imhof, T. Demiray and M. Morari, "Stabilization of Large Power Systems Using VSC–HVDC and Model Predictive Control," in *IEEE Transactions on Power Delivery*, vol. 29, no. 1, pp. 480-488, Feb. 2014.

[15] A. Mitra and D. Chatterjee, "Active Power Control of DFIG-Based Wind Farm for Improvement of Transient Stability of Power Systems," in *IEEE Trans. on Power Systems*, vol. 31, no. 1, pp. 82-93, Jan. 2016.

[16] Niloy P., Dheeman C. and Tanmoy B., "Transient Stability Improvement by Pre-fault and Post-fault modifications in Wind Power Plant Control", 1st international Conference on Large-Scale Grid Integration of Renewable Energy, India.

http://regridintegrationindia.org/wp-content/uploads/sites/3/2017/09/ 11C_4_GIZ17_143_paper_Niloy_Patari.pdf (cited on July 2018)

[17] P. W. Sauer, M. A. Pai and Chow J. H., " Power System Dynamics and Stability," 2nd ed., Wiley-IEEE press, USA, 2017.

[18] V. Shahu, T. Bandaru, T. Bhattacharya and D. Chatterjee, "Control of hybrid modular multilevel converter based HVDC system under DC short circuit faults," *IECON 2017*, Beijing, 2017, pp. 171-176.

[19] M. O. Faruque, Yuyan Zhang and V. Dinavahi, "Detailed modeling of CIGRE HVDC benchmark system using PSCAD/EMTDC and PSB/SIMULINK," in *IEEE Trans on Power Delivery*, vol. 21, no. 1, pp. 378-387, Jan. 2006.